Journal of Marine Science and Technology

Volume 28 | Issue 6 Article 10

A Study on Hydrodynamic Forces Induced by Liquid Tank of Lng Carrier in Waves Based on Experiment and Recurrent Neural Network

Van Minh Nguyen
Department of Naval Architecture and Marine Engineering, Changwon, Korea

Thi Thanh Diep Nguyen
Department of Naval Architecture and Marine Engineering, Changwon, Korea

Hyeon Kyu Yoon
Department of Naval Architecture and Marine Engineering, Changwon, Korea, hkyoon@changwon.ac.kr

A Study on Hydrodynamic Forces Induced by Liquid Tank of Lng Carrier in Waves Based on Experiment and Recurrent Neural Network

Acknowledgements

This research was supported by Basic Science Research Program through the National Research Foundation of Korea (NRF) funded by the Ministry of Science and ICT (2019R1F1A1057551).

Journal of Marine Science and Technology, Vol. 28, No. 6, pp. 548-563 (2020)
DOI: 10.6119/JMST.202012_28(6).0010

A STUDY ON HYDRODYNAMIC FORCES INDUCED BY LIQUID TANK OF LNG CARRIER IN WAVES BASED ON EXPERIMENT AND RECURRENT NEURAL NETWORK

Van Minh Nguyen, Thi Thanh Diep Nguyen and Hyeon Kyu Yoon

Key words: Recurrent Neural Network, sloshing load, model test.

ABSTRACT

The sloshing of liquid in a partially filled tank is of great concern to aerospace vehicles, road vehicles and ships due to complex nonlinear motion involving the free surface of the liquid. Sloshing is a type of violent liquid motion that is created by forces such as an impact and breaking waves. Oscillation of the liquid in the vessel may threaten navigation safety. This paper attempts to predict the hydrodynamic forces induced by the motion of liquid inside a tank based on experiment and Recurrent Neural Network (RNN). The experiment of sloshing test is carried out using the Stewart platform at Changwon National University (CWNU). The motions of the LNG carrier are inputted into the Stewart platform, then the hydrodynamic forces induced by the liquid in the tank are analyzed. Then, an RNN is used to model the complex dynamics of the sloshing load in the liquid tank and the RNN predictions are compared with the experimental results. This new approach, which offers robust modeling of the complex dynamics of a sloshing load in an LNG carrier, can be applied to simulate the ship maneuvering in waves.

I. INTRODUCTION

The ship maneuvering in waves has always been a challenging topic in the realm of ship hydrodynamics. The ability to accurately predict the maneuverability of a ship in waves would influence not only navigation safety, but also the economics of the ship's operation in adverse weather conditions. When an LNG carrier moves in waves, the maneuverability of the vessel can be significantly affected by the coupling dynamic of liquids and the ship dynamics in waves. Wave drift forces are the dominant influence on the trajectory of a ship in waves, while the hydrodynamic forces induced by the liquid may lead to extra forces on the ship. The motion of liquid in a partially filled tank in an LNG carrier has great concerns in a variety of engineering problems due to the effect of the free surfaces. Undesirable dynamic behaviors can occur due to sloshing load. Hence, the dynamic characteristics of the sloshing liquid should be analyzed and an accurate mathematical model of the sloshing load should be developed. Conventional experiments are still a reliable means of estimating the actual dynamic characteristics of a sloshing liquid. Therefore, it is necessary to estimate the hydrodynamic forces that are induced by the motion of the liquid inside a tank being carried by a ship in waves. Many researchers have performed sloshing analyses on liquid cargo and floating structures. The characterization and the theoretical studies of the sloshing problem originated with several different researchers (Faltinsen, 1978; Faltinsen and Timoka, 2001, 2002). Many studies have examined sloshing using different excitations and filling rates for liquid in two-dimensional (2D) tanks (Antuono et al., 2012; Elahi et al., 2015; Sahin and Bayraktar, 2015; Strand and Faltinsen, 2017). The influence of liquid level and excitation direction on nonlinear sloshing of a liquid in three-dimensional (3D) tanks have also been discussed in detail (Hwang et al., 1992; Liu et al., 2008; Wu et al., 2013; Hyeon and Cho, 2015). Previous studies showed that the resonant modes of the tanks are strongly related to the types of sloshing waves, such as planar waves and swirling waves. In marine applications, the hydrodynamic forces induced by the liquid in the tank may lead to extra forces on the ship as the ship moves in waves. The effect of liquid sloshing on the motion of LNG carriers has been addressed by several researchers (Kim et al., 2002; Kim et al., 2007; Nasar et al., 2008; Mitra et al., 2012; Nam et al., 2012). In most of these studies, the sloshing load inside a partially filled tank was estimated using the linearized potential flow, which assumes small-amplitude motions and inviscid and incompressible fluid.

All of the above mentioned approaches have some limitations

Paper submitted 06/01/20; revised 09/21/20; accepted 12/01/20. Corresponding Author: Hyeon Kyu Yoon (e-mail: hkyoon@changwon.ac.kr)
Department of Naval Architecture and Marine Engineering, Changwon, Korea

Table 1. Principal dimensions of the membrane tank

Item	Unit	Symbol	Real	Scale
Scale ratio	-	λ	1	1/70.993
Length	m	*L*	43.40	0.612
Breadth	m	*B*	37.97	0.535
Height	m	*H*	27.12	0.382

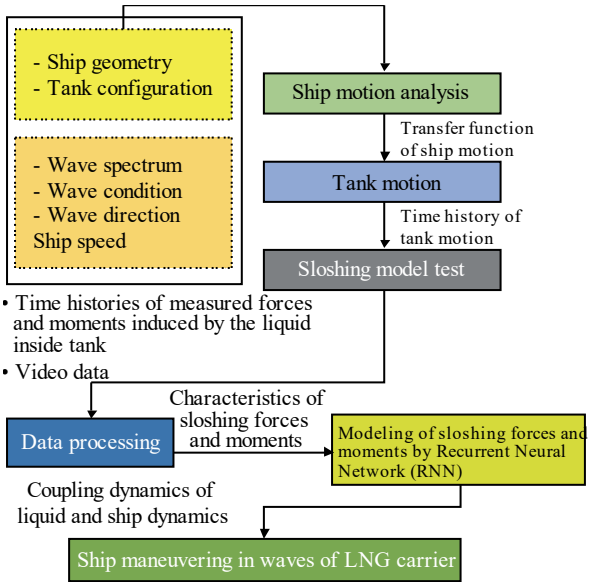

Fig. 1. Flowchart showing the coupling dynamics of liquid and ship dynamics of the LNG carrier

because most LNG carriers have adopted membrane-type LNG cargo systems and the sloshing forces in a 3D tank can be larger at the natural frequency of the tank, especially in a tank excited at resonant frequencies. This provided the motivation for the present research. The objective of this study is to investigate the hydrodynamic forces induced by the liquid inside a 3D membrane tank. First, an sloshing test of the liquid in a 3D membrane tank is conducted using the Stewart platform at CWNU to measure the hydrodynamic forces induced by the liquid inside the membrane tank. The effect of the filling rate and the motion responses of the LNG carrier to the hydrodynamic forces induced by the liquid in the tank are analyzed and discussed. Second, we propose an RNN and apply it to model the complex dynamics of a sloshing load in a tank because the combination of the ship's dynamics, the sloshing load and the coupled dynamic system require a complicated mathematical model. The RNN predictions are then compared with the experimental results. This new approach can provide a robust modeling platform for the complex dynamics of a sloshing load. This new approach to quickly and accurately simulating a sloshing load that is subject to the random motion of an LNG carrier can be applied to simulate the ship maneuvering in waves.

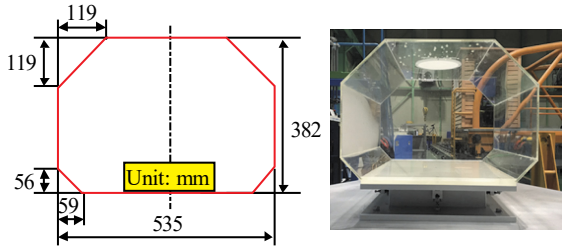

Fig. 2. Model of the membrane tank of the LNG carrier

II. EXPERIMENT

1. Experimental method

In this experiment, the tank is a scaled model of the membrane tank of an LNG carrier. The length, breadth and height of the model tank are 0.612, 0.535 and 0.382 m, respectively. Table 1 lists the dimensions of the real and scale model membrane tanks. The tank which was used in this experiment is the No. 3 tank of a 138000 m^3 LNG carrier. The coupling dynamic of the liquid and the ship dynamics of the LNG carrier in waves are shown in Fig. 1. The motion of the LNG carrier in waves is estimated by a three dimensional panel program (ANSYS-AQWA). Then, the time history of the tank is generated by the Stewart platform. Therefore, the time histories of the hydrodynamic forces induced by the liquid inside the tank are measured. Finally, the characteristic of the liquid inside the tank under forced motion is discussed.

2. Test conditions

According to the ITTC recommendations (2017), for a conventional LNG carrier with a membrane tank, the filling rate range from 10-70% of the tank's height because a very large sloshing impact occurs under the partially filled condition. Therefore, the experiment was carried in two filling conditions, 25% filling rate and 50% filling rate, gain a clear understanding of the sloshing forces due to the liquid in the partially filled tank. A series of model tests were conducted on the Stewart platform at CWNU to investigate the free surface elevation and the hydrodynamic forces induced by the liquid inside the membrane tank under the two different filling rates, and the membrane tank was subjected to the forced harmonic motion and the random motion of the tank. The membrane tank is made of transparent acrylic to allow observation of the flow motion inside the tank, as shown in Fig. 2. For harmonic motion, 1 degree of freedom (DOF) forced motion of the tank is represented using Eq. (1).

$$\eta(t) = \eta_0 \sin(2\pi f t) \tag{1}$$

Where η, f and t are the amplitude of the forced motion of the tank, the frequency of the motion and the time, respectively. On the other hand, the random motion of the membrane tank is represented as the motion of the membrane tank generated by an irregular wave. The random motion in the time domain

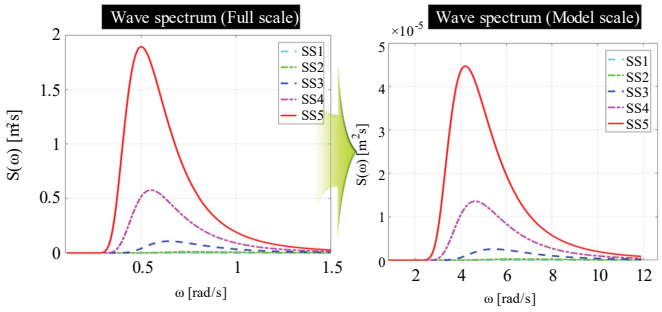

Fig. 3. Wave spectrum of the full scale and model scale tanks

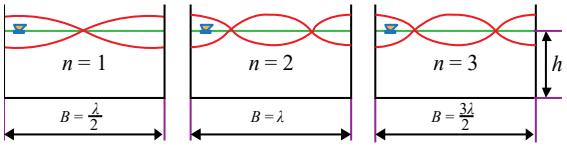

Fig. 4. Mode of the natural frequency of the rectangular tank

can be estimated by Eq. (2). The wave amplitude can be expressed in a wave spectrum by Eq. (3). The ITTC spectrum is used to estimate the random motion of the membrane tank. Fig. 3 illustrates the estimation of the wave spectrum in the full scale and model scale membrane tanks.

$$\eta(t)=\sum_{i=1}^{N} RAO_i \zeta_{a_i} \cos\left(\omega_i t+\varepsilon_i+\varepsilon_{\eta i}\right) \tag{2}$$

$$\zeta_{a_i}=\sqrt{2S(\omega_i)\Delta\omega} \tag{3}$$

where, $S(\omega)=\frac{A}{\omega^5}e^{-B/\omega^4}$, $A=173\frac{H_{1/3}^2}{T^4}$ and $B=\frac{691}{T^4}$ ζ_{a_i}, ω_i, k_i, ε_i, $H_{1/3}$, T and $S(\omega)$ are the wave amplitude component, the wave frequency component, the wave number component, the random phase angle component, the significant wave height and the mean wave period, respectively.

$$\omega^2=kg\tanh(kh) \tag{4}$$

$$\omega=\sqrt{\frac{2\pi}{\lambda}g\tanh\left(\frac{2\pi}{\lambda}h\right)} \tag{5}$$

$$B=\frac{n}{2}\lambda\rightarrow\lambda=\frac{2}{n}B \tag{6}$$

$$\omega_{rec}=\sqrt{\frac{2\pi}{\frac{2}{n}B}g\tanh\left(\frac{2\pi}{\frac{2}{n}B}h\right)}=\sqrt{g\frac{n\pi}{B}\tanh\left(\frac{n\pi}{B}h\right)} \tag{7}$$

Table 2. Natural frequency of the membrane tank

Mode	f_{surge} [Hz]		f_{sway} [Hz]	
	25%	50%	25%	50%
1	0.76	0.98	0.86	1.09
2	1.39	1.57	1.53	1.69
3	1.86	1.95	2.02	2.09

Table 3. Test conditions for harmonic motion

Forced motion	Frequency [Hz]	Amplitude of motion [mm] or [°]
Surge	0.2 ~ 2.2 (Interval of 0.2)	20
Sway		20
Yaw		2

The dispersion relation for the wave elevation inside the partially filled tank can be written using Eq. (4). By replacing the wave number with the wavelength on the right hand side of Eq. (4), the frequency of the tank can be rewritten as Eq. (5). Fig. (4) shows the relationship between the wavelength and the breadth of the rectangular tank. The wavelength can be estimated by Eq. (6). Solving Eq. (5) by replacing Eq. (6) with Eq. (5), the natural frequency of the rectangular tank can be directly obtained by Eq. (7). Therefore, the natural frequency for the surge and sway of the rectangular tank are estimated by Eqs. (8)-(9). Then, the natural frequency of the membrane tank is estimated by Eq. (10). A correction of the natural frequency of the membrane tank which is estimated based on the natural frequency of the rectangular tank is suggested by Faltinsen and Timoka (2009). The result of the natural frequencies of the membrane tank are listed in Table 2.

$$\omega_{surge}=\sqrt{g\frac{n\pi}{L}\tanh\left(\frac{n\pi h}{L}\right)} \tag{8}$$

$$\omega_{sway}=\sqrt{g\frac{n\pi}{B}\tanh\left(\frac{n\pi h}{B}\right)} \tag{9}$$

$$\frac{\omega_{corr}^2}{\omega_{sway}^2}=1-\frac{\frac{\delta_1}{\delta_2}\sinh^2\left(\pi n\frac{\delta_2}{B}\right)-\frac{\delta_1}{\delta_2}\sin^2\left(\pi n\frac{\delta_1}{B}\right)}{\pi n\sinh\left(2\pi n\frac{h}{B}\right)} \tag{10}$$

where L is the tank length, B is the tank breadth, h is the height of the water inside the tank, g is the acceleration due to gravity, n is the mode of the motion, and δ_1 and δ_2 are the horizontal and vertical dimensions of the tank's chamfer, respectively.

In this experiment, the range of frequency was chosen the

Table 4. Test conditions for random motion

Forced motion	Range of frequency [Hz]	Number of frequency [-]	Sea state
Surge	0.2~2.2	200	3,4

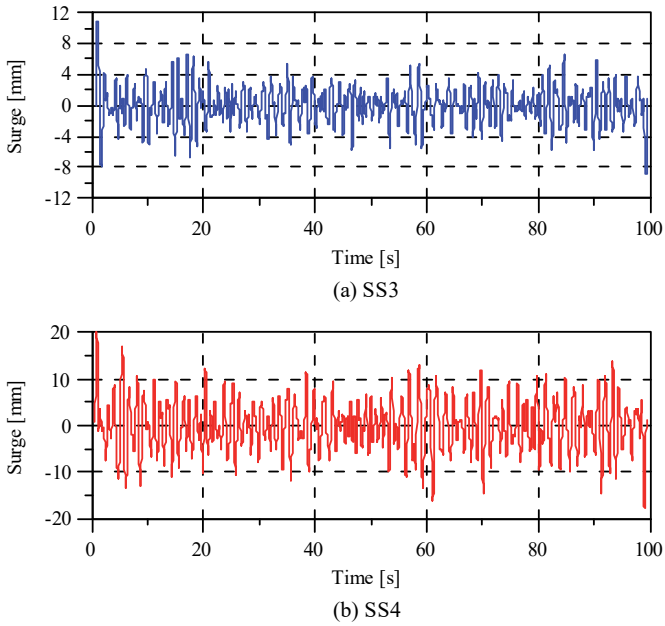

Fig. 5. Time series of the random surge in irregular wave

wave spectrum and the natural frequency of the membrane tank. The test conditions for harmonic motion are listed in Table 3. In addition, three frequencies of the motion of the tank near the natural frequencies of the tank are examined. The test condition for random motion are listed in Table 4. Fig. 5 shows the random motion of the surge in the time domain at sea state 3 (SS3) and sea state 4 (SS4).

3. Experimental setup

Two filling rates of the membrane tank were examined and the tank was moved by different types of external excitation, such as surge, sway and yaw. The experimental setup is shown in Fig. 6. The measurement instruments used in the experiment are a load cell and IMU (inertia measurement unit) device; these were used to measure the hydrodynamic forces induced by the liquid inside the tank and the motion generated by the Stewart platform. The load cell is installed between the Stewart platform and the membrane tank. The IMU device is installed under the surface of the Stewart platform. Two GOPRO cameras are installed in the x and y directions of the tank to capture the motion of water inside the tank in the x and y directions during excitation.

4. Data analysis

The motion of the liquid inside the tank will produce the

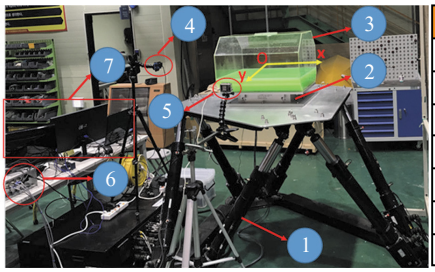

No	Item
1	Stewart platform
2	Load cell
3	Sloshing tank
4	Camara in x direction
5	Camara in y direction
6	Amplifier
7	Host computer

Fig. 6. Experimental setup of the sloshing test at 25% filling rate

different flow phenomenon under the forced motion and snapshots of the wave elevation along the tank wall is analyzed by the capture image from two cameras. The maximum sloshing peak for each excitation frequency is estimated to analyze the effect of excitation on the hydrodynamic forces induced by the liquid inside the tank. The hydrodynamic forces and moment are non-dimensionalised using Eqs. (11)-(13).

$$X' = \frac{X}{\rho g h^2 B} \tag{11}$$

$$Y' = \frac{Y}{\rho g h^2 B} \tag{12}$$

$$N' = \frac{N}{\rho g h^2 B^2} \tag{13}$$

where X, Y and N are the surge force, sway force and yaw moment, respectively. B and h are the breadth of the tank and the height of water inside the tank, respectively. ρ is the water density and g is the gravity acceleration.

III. RECURRENT NEURAL NETWORK (RNN)

1. RNN modeling

In the fourth industrial revolution, artificial intelligence (AI) has been widely used in various applications because AI can produce the desired output even in cases that lack information. A recurrent neural network (RNN) is a class of neural networks that consider the sequence of the input data. RNN is used for specific problems, such as speech recognition, language modeling and forecasting. In addition, RNN has gradually advanced, such that they now achieve the best predictive power in various engineering applications. RNN relies on a distributed hidden state that allows them to efficiently store a great deal of information about past states. In addition, an RNN can be used to model nonlinear dynamic behavior, allowing them to update their hidden states in complicated ways. Construction of a mathematical model of a sloshing load subject to the random motion of an LNG carrier is a challenging and difficult problem. This is because the nonlinear characteristics of a sloshing liquid sloshing are due to the effects of the free surfaces.

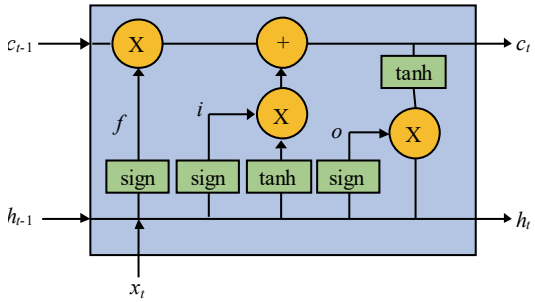

Fig. 7. Diagram of an LSTM's structure

Therefore, a novel RNN is herein applied to model the complex dynamics of the sloshing load in a liquid tank subject to the arbitrary motion of an LNG carrier. In a traditional multilayer perceptron neural network, all inputs are independent of each other, while in an RNN, this is not the case. The value of a hidden state at any given point in time, t, is calculated based on the value of the input at the current time step and the value of the hidden state at the previous time step. h_t and h_{t-1} are the values of the hidden state at times t and $t-1$, respectively, x_t is the value of the input at time t. The output value y_t at time t is the product of the weight matrix W and the hidden state h_t with *softmax*. The long-short term memory (LSTM) method avoids the exploding gradient and vanishing gradient problems that often occur in traditional RNN (Hochreiter and Schmidhuber, 1997). An LSTM implements recurrence in a similar manner as a the traditional RNN. However, an LSTM has four layers that interact in a very specific way. Fig. 7 illustrates the transformations applied to the hidden state at time t in an LTSM. c, i, f and o are the cell state, input gate, forget gate and output gate, respectively. Input gate i, output gate o and forget gate f can be estimated using Eqs. (14)-(16). The input gate i is employed to control the output of the memory cell into the visible state h_t via the output gate o. The forget gate f is used to determine what should be forgotten by the memory cell c_t. The parameters of these gates are learned using a set of training data. The memory cell c_t evolves through addition of inputs from the forget and input gates, as estimated using Eq. (17).

$$i = \sigma\left(W_i h_{t-1} + U_i x_t\right) \tag{14}$$

$$f = \sigma\left(W_f h_{t-1} + U_f x_t\right) \tag{15}$$

$$o = \sigma\left(W_o h_{t-1} + U_o x_t\right) \tag{16}$$

$$c_t = \left(c_{t-1} \bullet f\right) + \left(i \bullet \tanh\left(W_o h_{t-1} + U_h x_t\right)\right) \tag{17}$$

$$h_t = \tanh\left(c_t\right) \bullet o \tag{18}$$

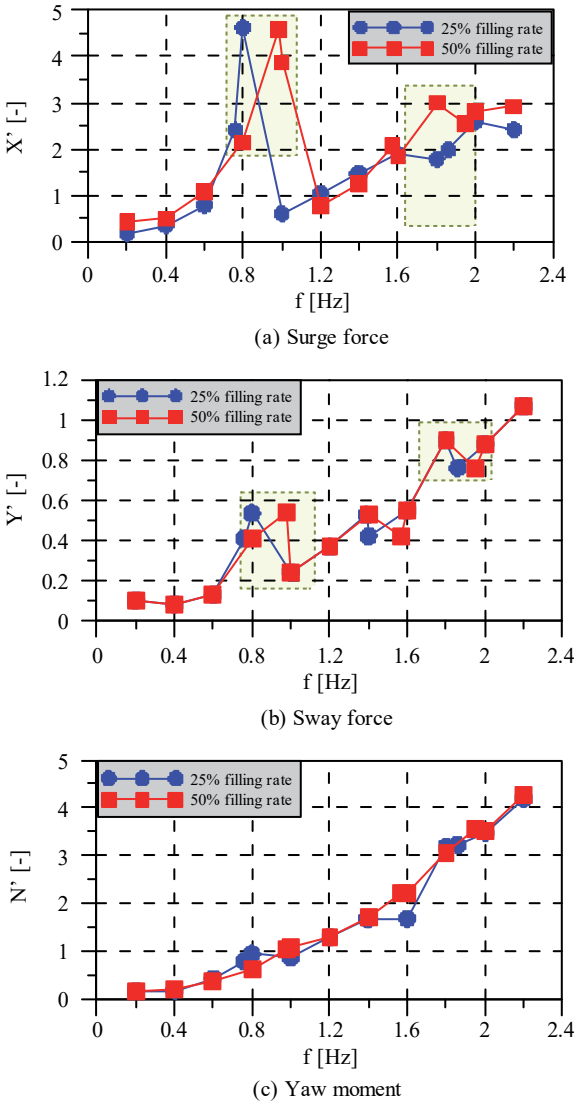

Fig. 8 Non-dimensional hydrodynamic forces in forced surge

2. Data collection and evaluation of the RNN

The time series of the training data used to train the network are obtained from the experimental results. The training data consists of information about the motion of the LNG carrier and the sequence of the hydrodynamic forces induced by motion of the liquid in the tank at the previous time point, while the output of the training data is information about the hydrodynamic forces induced by motion of the liquid in the tank at the current time point. For a given time series, the training data are normalized to range from 0 to 1 to train the proposed RNN. The LSTM model is applied to predict the nonlinear hydrodynamic forces induced by the liquid in harmonic and random motion. The predicted hydrodynamic forces induced by the liquid inside the tank are estimated using the sequential motion of the tank and the sloshing load at the previous time point. The mean square error (MSE) is employed as the objective function to be minimized during LSTM training.

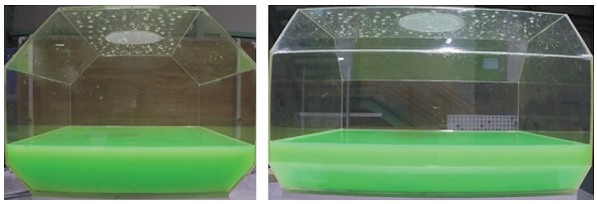

(a) f = 0.2 Hz

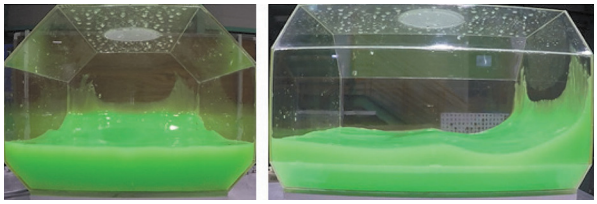

(b) f = 0.6 Hz

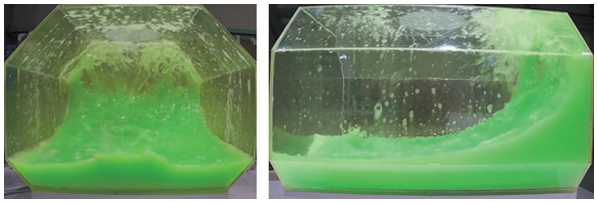

(c) f = 0.8 Hz

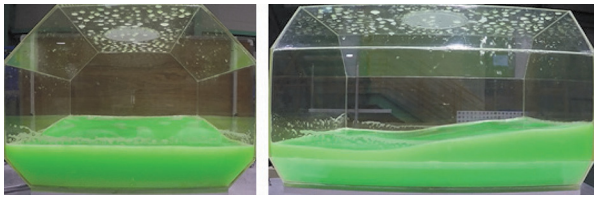

(d) f = 1.0 Hz

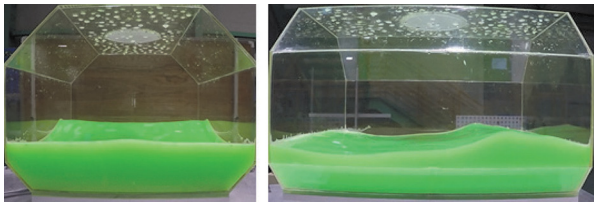

(e) f = 1.4 Hz

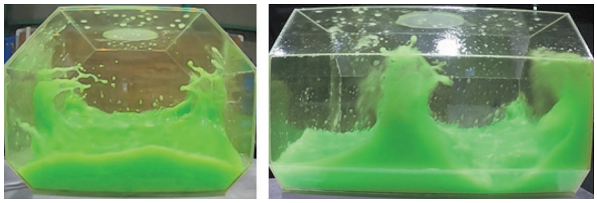

(f) f = 1.8 Hz

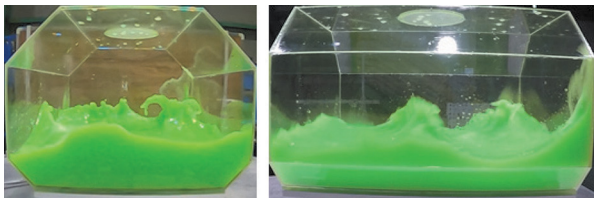

(g) f = 2.2 Hz

Fig. 9 Wave elevation at 25% filling rate in forced surge (Left: camera in x direction, Right: camera in y direction)

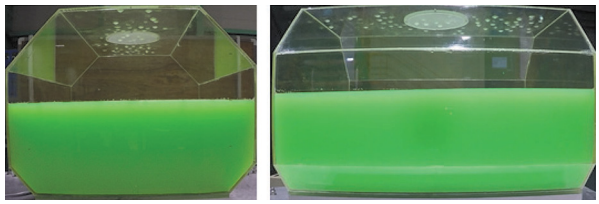

(a) f = 0.2 Hz

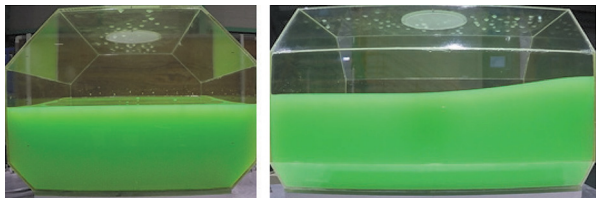

(b) f = 0.6 Hz

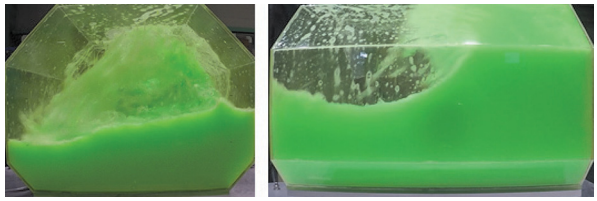

(c) f = 1.0 Hz

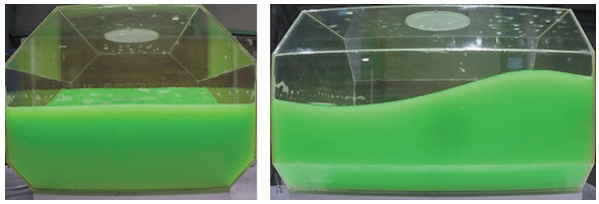

(d) f = 1.4 Hz

(e) f = 1.8 Hz

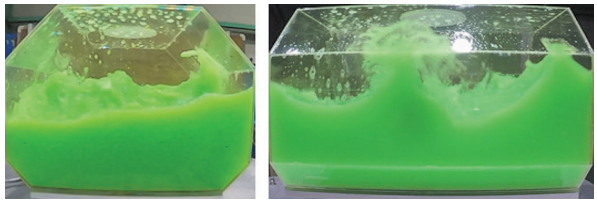

(f) f = 2.2 Hz

Fig. 10 Wave elevation at 50% filling rate in forced surge (Left: camera in x direction, Right: camera in y direction)

IV. RESULTS AND DISCUSSION

1. Hydrodynamic forces induced by water in forced surge

Fig. 8 shows the hydrodynamic forces induced by the liquid tank at both filling rates in forced surge. A large amount of sloshing occurs when the excitation frequency is in the vicinity of the natural frequencies of the tank. The 1st maximum surge force occurs near the 1st natural frequency of the tank, while

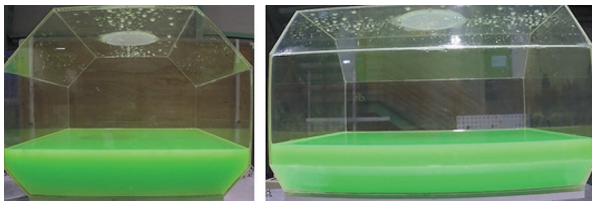
(a) f = 0.2 Hz

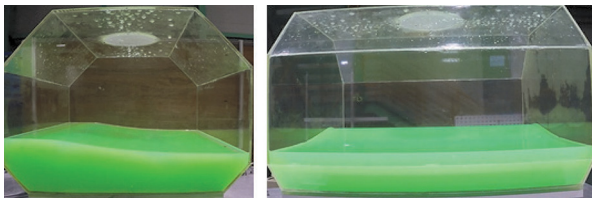
(b) f = 0.6 Hz

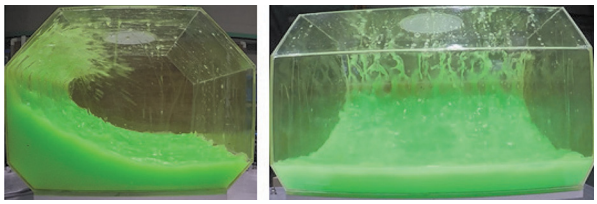
(c) f = 1.0 Hz

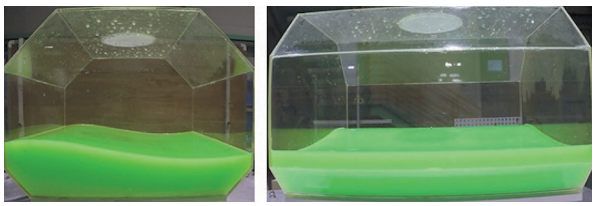
(d) f = 1.4 Hz

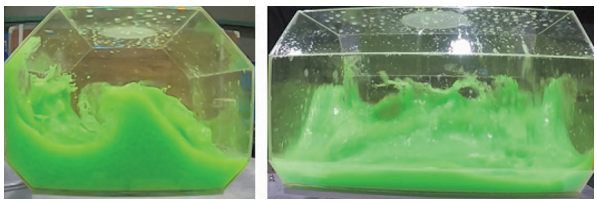
(e) f = 1.8 Hz

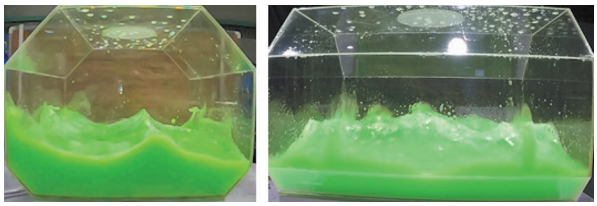
(f) f = 2.2 Hz

Fig. 11 Wave elevation at 25% filling rate in forced sway (Left: camera in x direction, Right: camera in y direction)

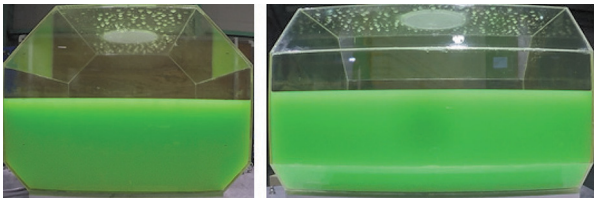
(a) f = 0.2 Hz

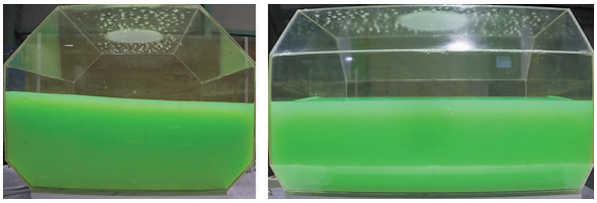
(b) f = 0.6 Hz

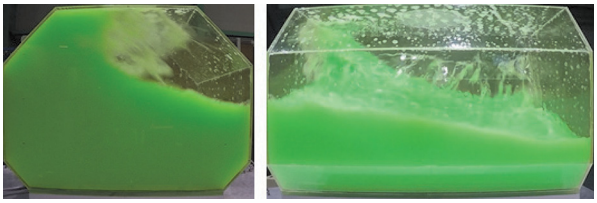
(c) f = 1.0 Hz

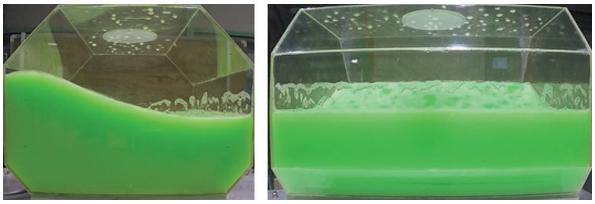
(d) f = 1.4 Hz

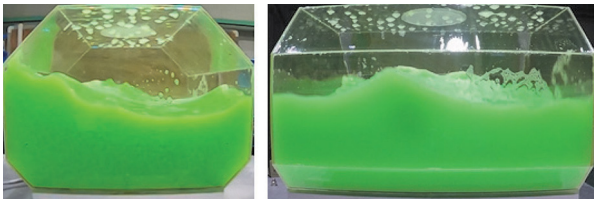
(e) f = 1.8 Hz

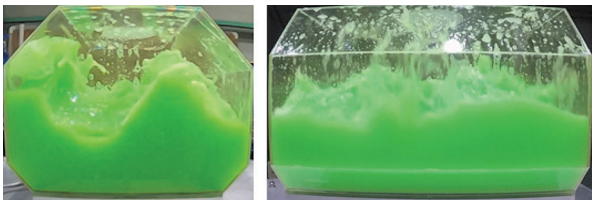
(f) f = 2.2 Hz

Fig. 12 Wave elevation at 50% filling rate in forced sway (Left: camera in x direction, Right: camera in y direction)

the 2nd maximum surge force occurs near the 3rd the natural frequency of the tank. The maximum value of the surge force is the same, but it is shifted by the different resonant frequencies of the filling rates. Interestingly, sway force also occurs in forced surge, and the sway force gradually increases in strength when the excitation frequency increases. The 1st and 2nd peaks of the sway force occur near the 1st and 3rd natural frequencies of the tank, respectively. This is because the breadth and length of the membrane tank are almost the same, which generates swirling. The yaw moment also gradually increases as the excitation frequency increases. Figs. 9–10 show the wave elevation in forced surge in the x and y directions at filling rates of 25% and 50%, respectively. The wave elevation is captured when the amplitude of the excitation of the tank is

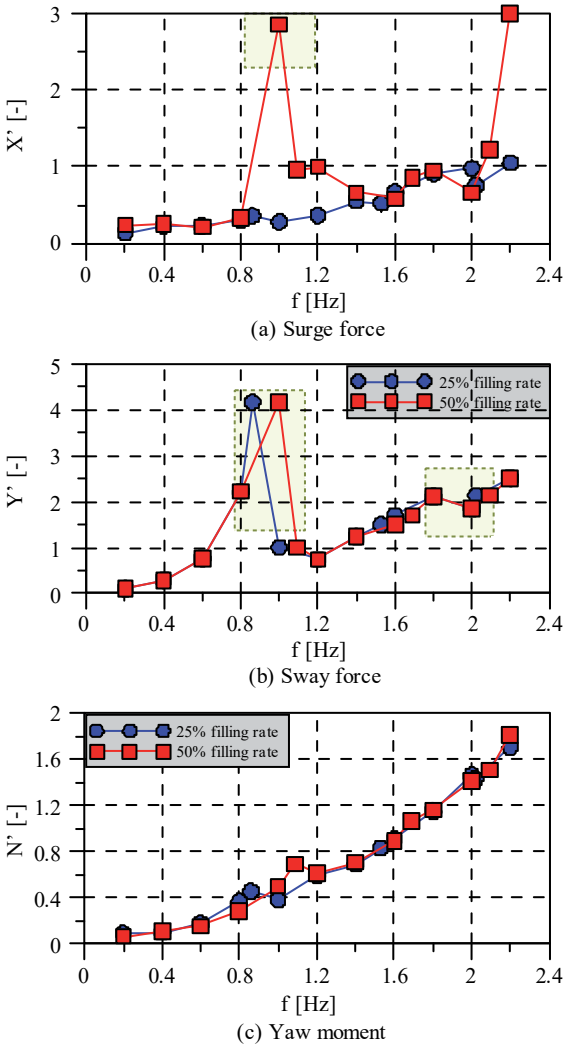

Fig. 13 Non-dimensional hydrodynamic forces in forced sway

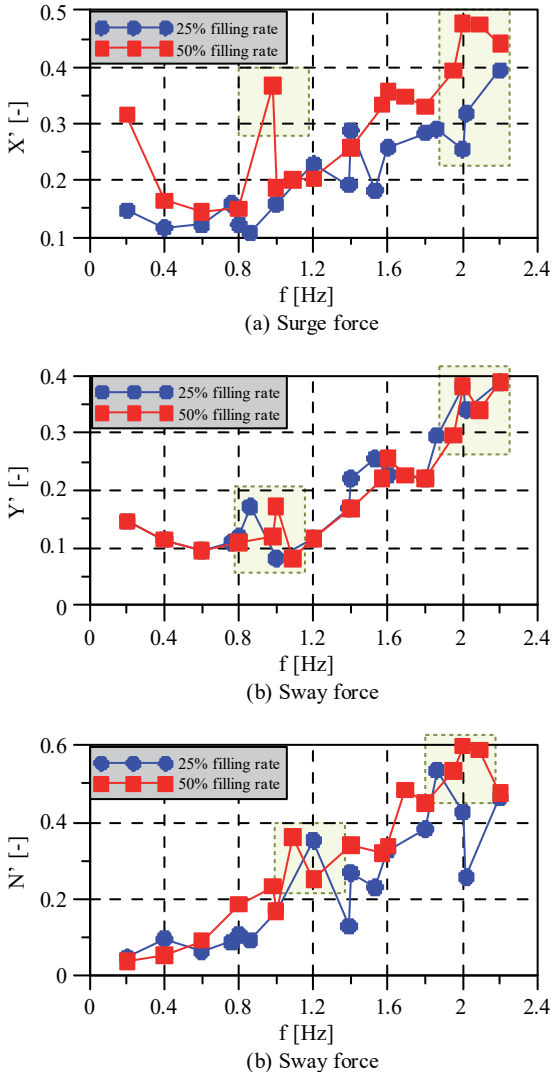

Fig. 14 Non-dimensional hydrodynamic forces in forced yaw

at a maximum. The wave appears and travels only in the excitation direction of the tank at a small excitation frequency. However, when the excitation frequency is in the vicinity of the natural frequency of the tank (0.6, 0.8 and 1.8 Hz), the wave appears and travels perpendicular to the excitation direction of the tank. The water level increases dramatically when the excitation frequency is close to the natural frequency of the tank. In addition, the swirling phenomenon occurs, as does the run-up phenomenon in the corners of the tank. In this case, the movement causes not only the surge force, but also an increase in the sway force, which becomes large and generates swirling, as seen in Figs. 9c, 9f, 10c and 10f.

2. Hydrodynamic forces induced by water in forced sway

Figs. 11–12 show the wave elevation in forced sway in the x and y directions at filling rates of 25% and 50%, respectively. The wave elevation is captured when the amplitude of excitation motion reaches a maximum. The wave appears and travels only in the excitation direction of the tank at a small excitation frequency.

When the excitation frequency is in the vicinity of the natural frequency of the tank (1.0 and 2.0 Hz), the wave appears and travels perpendicular to the excitation direction of the tank. The water level increases dramatically, and water hits the roof of the tank when the excitation frequency is in the vicinity of the natural frequency of the tank. In addition, the swirling phenomenon occurs, causing two different water levels and leading to the run-up phenomenon in the corners and middle of the tank. In this case, the amount of water at the 50% filling rate is larger than that at the 25% filling rate due to the effect of the tank's chamfer plate, as shown in Figs. 11c and 12c.

Fig. 13 shows the hydrodynamic forces induced by the liquid in the tank at the two filling rates in forced sway. The sloshing force is dominated by the excitation of the tank when the excitation frequency is in the vicinity of the natural frequencies of the tank. The 1st maximum sway occurs near the 1st natural frequency of the tank for forced sway, while the 2nd

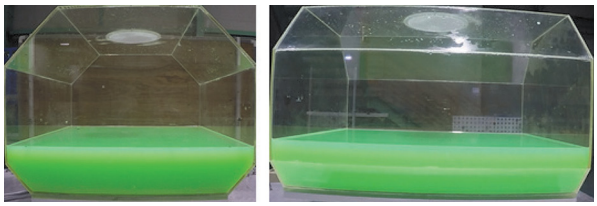
(a) f = 0.2 Hz

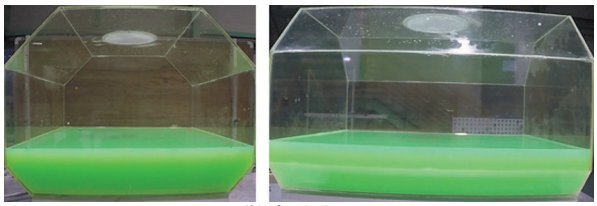
(b) f = 0.6 Hz

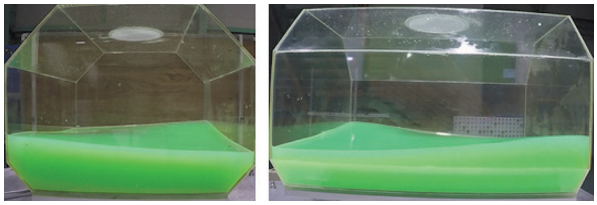
(c) f = 1.0 Hz

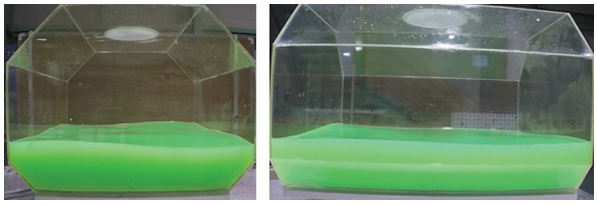
(d) f = 1.4 Hz

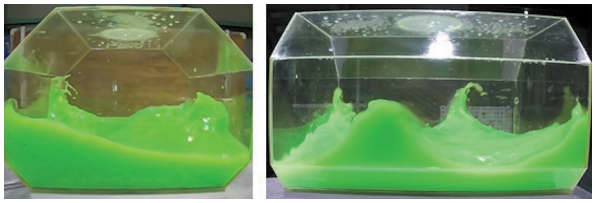
(e) f = 1.8 Hz

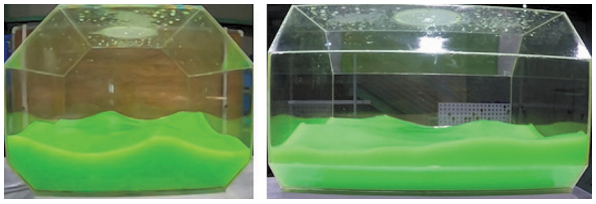
(f) f = 2.2 Hz

Fig. 15 Wave elevation at 25% filling rate in forced yaw (Left: camera in x direction, Right: camera in y direction)

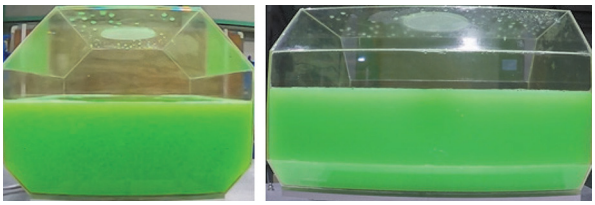
(a) f = 0.2 Hz

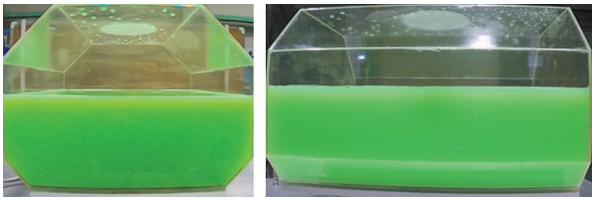
(b) f = 0.6 Hz

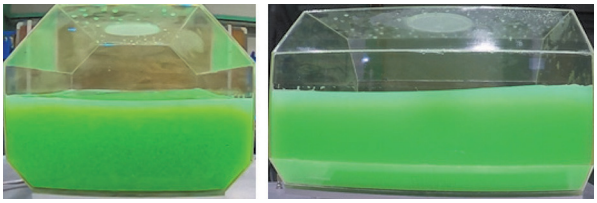
(c) f = 1.0 Hz

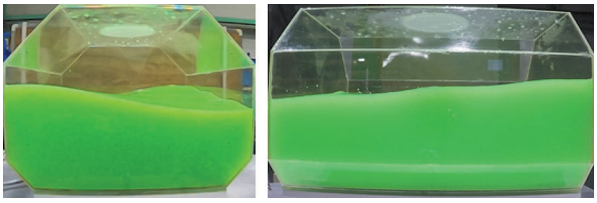
(d) f = 1.4 Hz

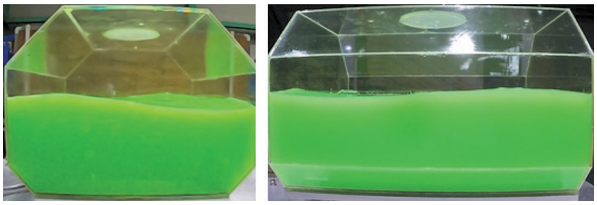
(e) f = 1.8 Hz

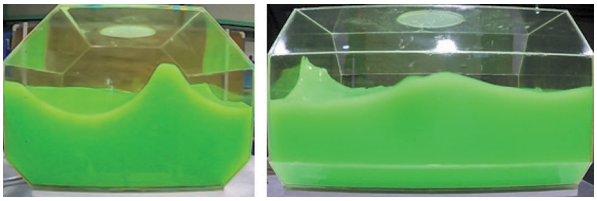
(f) f = 2.2 Hz

Fig. 16 Wave elevation at 50% filling rate in forced yaw (Left: camera in x direction, Right: camera in y direction

maximum sway force occurs near the 3rd natural frequency of the tank, as shown in Fig. 13. The maximum value of the sway force is the same but shifted by the resonant frequency at the two filling conditions. Interestingly, surge force also occurs in forced sway and gradually increases as the excitation frequency increases. The surge force at the 50% filling rate is larger than one at the 25% filling rate, and it reaches a peak when the excitation frequency is close to the 1st and 3rd natural frequencies of the tank for forced sway. This is because the swirling generated at a 50% filling rate is larger than that at 25%, as shown in Figs. 11c and 12c. In forced sway, the yaw moment also gradually increases as the excitation frequency increases.

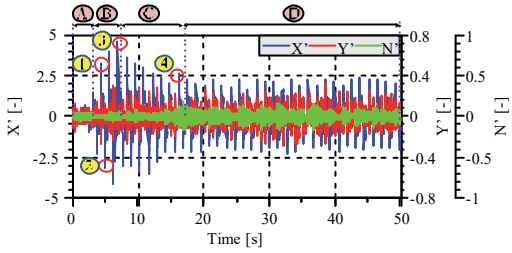

(a) Time series of the hydrodynamic forces in forced surge (25% filling rate)

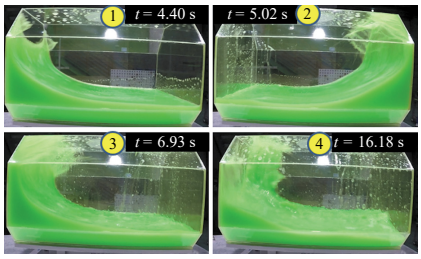

(b) Wave elevation in forced surge (25% filling rate)

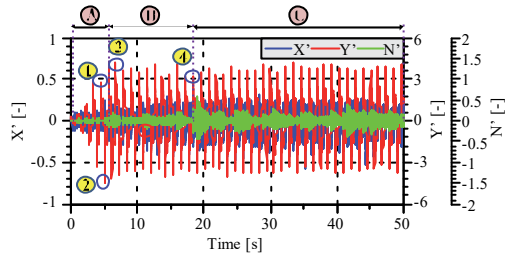

(c) Time series of the hydrodynamic forces in forced sway (25% filling rate)

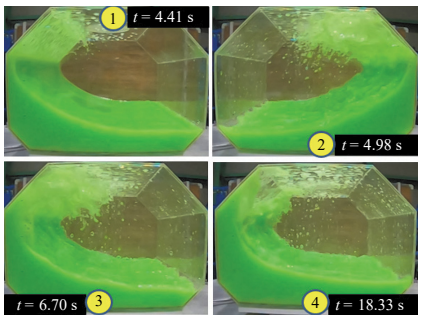

(d) Wave elevation in forced sway (25% filling rate)

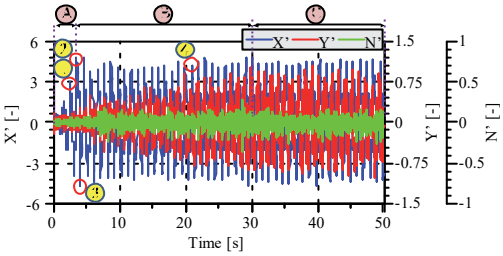

(e) Time series of the hydrodynamic forces in forced surge (50% filling rate)

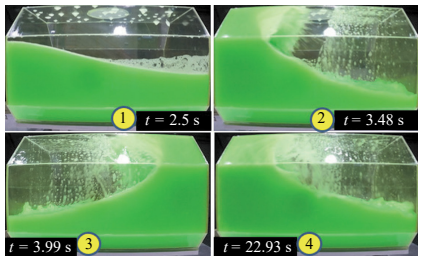

(f) Wave elevation in forced surge (50% filling rate)

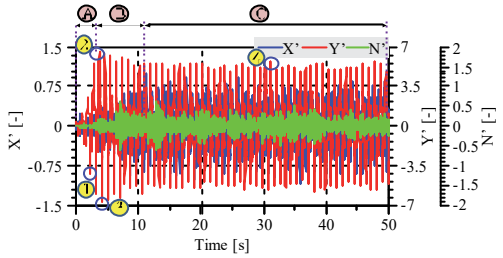

(g) Time series of the hydrodynamic forces in forced sway (50% filling rate)

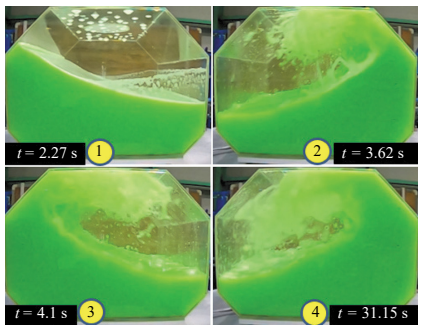

(h) Wave elevation in forced sway (50% filling rate)

Fig. 17 Time series of the hydrodynamic forces and wave elevation

3. Hydrodynamic forces induced by water in forced yaw

Fig. 14 shows the hydrodynamic forces induced by the liquid in the tank at the two filling conditions in forced yaw. The yaw moment gradually increases as the excitation frequency increases; the maximum yaw moment is coupled with the surge force and the sway force. The yaw moment is dominated when the excitation frequency is approximately equal to the natural frequency of the tank in forced surge and forced sway. The surge force and sway force are closely related to the wave elevation and increase dramatically as the excitation frequency increases. Figs. 15–16 show the wave elevation in forced yaw at filling rates of 25% and 50%, respectively. The coupling motion of surge and sway of the 3D membrane tank is investigated. The wave elevation is captured when the amplitude of the excitation of the tank is at its maximum. The wave appears and travels only in the excitation direction of the tank at a small excitation frequency. When the excitation frequency is in the vicinity of the natural frequency of the tank (1.0 and 1.8 Hz), the run-up phenomenon occurs in the tank's corners and a wave appears and travels based on the direction of the excitation rotation.

4. Hydrodynamic forces induced by water under resonant excitation

In this section, the excitation frequencies are set to the corresponding natural frequencies of the membrane tank, i.e., 0.76 and 0.86 Hz. Fig. 17a shows the time histories of the hydrodynamic forces induced by the water when the excitation frequency approaches to the surge natural frequency of the tank. The largest discrepancy between the results can be seen in Fig. 17a, where the sway force and yaw moment occur. Given the result over time, the behavior of the water inside the tank can be divided into four phases, A, B, C and D. Phase A represents the sloshing in the tank that occurs when the surge changes rapidly over time. Then, the sway force and yaw moment begin to appear and increase dramatically because the surface of the water in the tank starts to rotate at phase B. This phenomenon is clearly visible in the movement of the water in the tank in Fig. 17b.

Next, the surge force begins to decrease as the sway force reaches a steady state in phase C, as shown in Fig. 17b. Finally, the yaw moment evens out and has the largest amplitude compared to the previous periods. This is because the water has been steadily rotating and the amplitude of the surge force and sway force do not change much. Moreover, the wave pattern for the sloshing and swirling phenomena can be visually observed in snapshots captured from the video recording.

Fig. 17b shows the wave in the natural frequency in forced surge at a 25% filling rate. A wave break appears and travels in the excitation direction of the tank at about 4.40 s. After 6.93 s, a swirling wave that is rotated anticlockwise (viewed from the top) is generated in the tank. From about 6.93 s to 16.18 s, the swirling waves increase the water level in the corners of the tank, which increases dramatically and hits the roof of the tank when the amplitude of excitation is at a maximum. Fig. 17c shows the time histories of the hydrodynamic forces induced by the water when the excitation frequency approaches to the sway natural frequency of the tank. The time histories of the hydrodynamic forces induced by the water reveal a larger discrepancy than the one in forced surge. The behavior of the water in the tank can be divided into three phases, A, B, and C. Phase A involves sloshing in the tank, which changes rapidly over time due to sway. Then, the surge force and yaw moment also occur because the internal fluid changes gradually and the flow becomes violent in phase B, as shown in Fig. 17c. Next, unlike the previous case, the force exerted in the direction of motion has not changed its amplitude after the appearance of swirling waves. Fig. 17d shows the transient waves captured in the time domain at a 25% filling rate in forced sway. The internal fluid changes gradually to a violent flow within two to three periods. Although a transient stage occurs, swirling waves dominate because the wave is perpendicular to the forced oscillation direction. When the tank is forced in the y direction, it is easy to trigger swirling waves, especially if the tank is excited by the resonant frequencies. As is evident in Fig. 17d, a rising flow occurs along the wall of the tank after a collision with the side wall, then the wave breaks and hits the roof of the tank at about 4.98 s. As a result, the water level increases dramatically in the corner of the tank from about 6.70 s to 18.33 s.

Fig. 17e shows the time histories of the hydrodynamic forces induced by the water when the excitation frequency approaches the sway natural frequency of the tank at a 50% filling rate. Similarly, the forces that change over time can be divided into three phases, including sloshing, rotating water, and swirling, which appear to change steadily over time. However, at a 50% filling rate, phase B takes place for a longer time than it does at 25% due to the increased volume of water. Fig. 17f shows the wave elevation at a 50% filling rate in forced surge. The wave begins at the left wall and increases dramatically from about 2.5 s to 3.99 s. The motion of the sloshing wave gradually catches up with the movement of the tank after collision with the roof of the tank. The surge force induced by the liquid is dominant when the liquid is the most violent, around 22.93 s.

Fig. 17g shows the time histories of the hydrodynamic forces induced by the water when the excitation frequency approaches the sway natural frequency of the tank at the 50% filling rate. The behavior of the hydrodynamic force is the same as that seen at the 25% filling rate. Fig. 17h shows the wave elevation captured at the 50% filling rate in forced sway. The water level increases at the left wall at about 2.27 s, then the wave break appears and travels in the excitation direction of the tank at about 3.62 s. Swirling occurs at the bounds of the top chamfers and the tank ceiling. After 6.93 s, a swirling wave that rotates anticlockwise (viewed from the top) is generated in the tank. From about 6.93 s to 16.18 s, the swirling waves increases the water level in the tank corners dramatically, hitting the roof of the tank as the amplitude of the excitation of the tank reaches a maximum. The wave breaks violently during transfer from sloshing to swirling after 31.15 s. These observations confirm that swirling can occur in the membrane tank as a consequence of forced motion. In this case, the fluid moving in the tank is almost bidirectional and the waves inside the tank are created almost parallel to the wall. Flow separation and rotation are obvious for the partially filled membrane tank.

5. Hydrodynamic forces induced by water in random motion

Next, sloshing under random motion is studied because the excitatory motion that causes sloshing under real sea conditions is generally irregular and includes many frequency components. Translation excitations corresponding to surge and sway motions are exerted on the membrane tank and the hydrodynamic forces that occur in response are considered in this study. Random motions are chosen to represent the ship motion induced in sea state 3 (SS3) and sea state 4 (SS4). Fig. 18 shows the time histories of hydrodynamic forces induced by liquid in a partially filled membrane tank under random excitation and different filling rates. The hydrodynamic forces change significantly depending on the sea conditions and filling

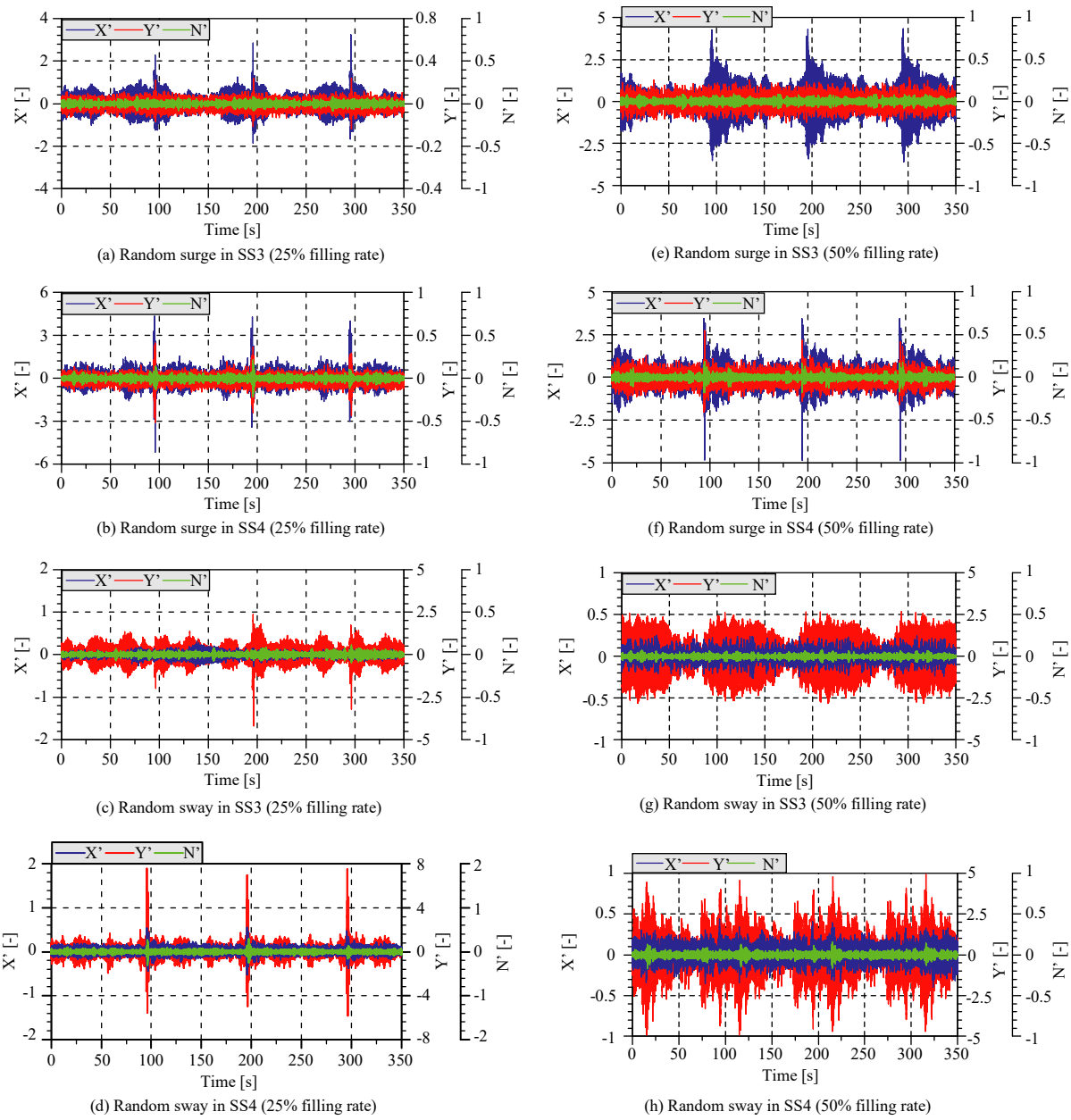

(a) Random surge in SS3 (25% filling rate)

(e) Random surge in SS3 (50% filling rate)

(b) Random surge in SS4 (25% filling rate)

(f) Random surge in SS4 (50% filling rate)

(c) Random sway in SS3 (25% filling rate)

(g) Random sway in SS3 (50% filling rate)

(d) Random sway in SS4 (25% filling rate)

(h) Random sway in SS4 (50% filling rate)

Fig. 18 Time series of the hydrodynamic forces in random motion

rate. In particular, variation in the filling rate causes the largest discrepancy in the hydrodynamic force induced by the water inside the membrane tank.

Fig. 19 shows the mean values of the top 33% peaks of the hydrodynamic force induced by the water in random surge and sway conditions, respectively. The statistical analysis shows that the hydrodynamic force induced by the liquid is two times greater under the same random motion conditions with a filling rate of 50% vs. 25%. This is because the greater volume of liquid exerts a stronger force. The relative differences for the random motion in surge and sway at the 25% filing rate are 24.63% and 15.22%, respectively. On the other hand, the relative differences for random motion in surge and sway at the 50% filing rate are 27.62% and 11.51%, respectively. These findings indicate that the hydrodynamic forces will be affected by filling rates more than the influence of sea conditions.

Exceedance probability can be calculated to predict the probable extreme values of the hydrodynamic forces of a sloshing load based on ITTC procedures (2017). Exceedance probability can be estimated after sorting the peak values of the hydrodynamic force induced by the liquid. Fig. 20 shows the exceedance probability distribution regarding the hydrodynamic forces induced by the liquid according to the filling rate and the sea conditions. Return period which occurs the extreme hydrodynamic force can be estimated based on the statistical analysis using an exceedance probability distribution.

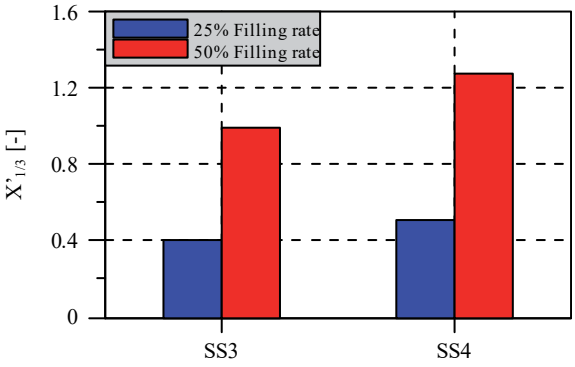

(a) Surge force in random surge

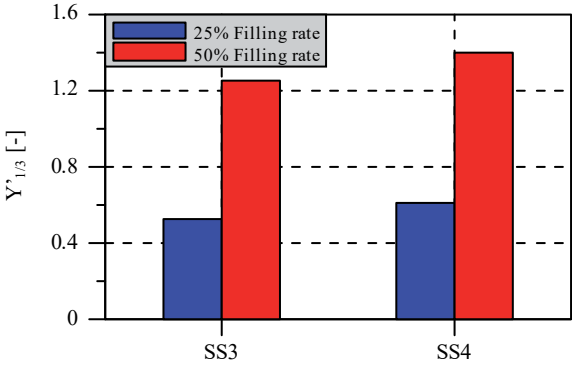

(b) Sway force in random sway

Fig. 19 Significant forces in random motion

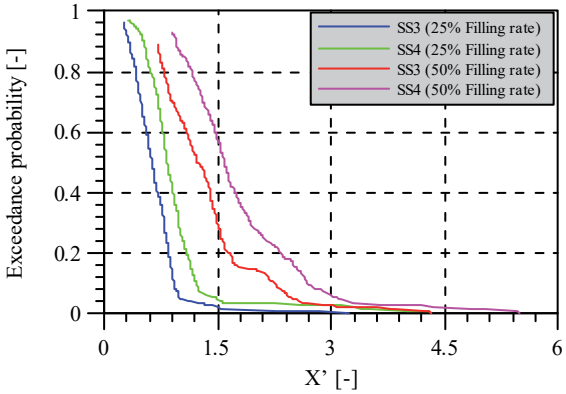

(a) Random surge

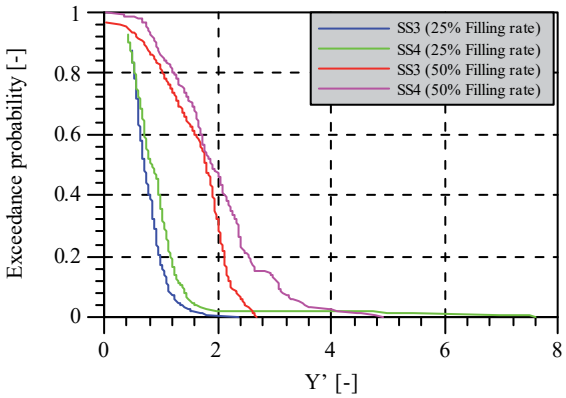

(b) Random sway

Fig. 20 Exceedance probability of the hydrodynamic forces

For random surge, the exceedance probability distribution of the surge force at SS4 with a 50% filling rate gradually shifted to the right compared to the other sea condition and filling rate, as shown in Fig. 20a. This suggests that the surge force at a 25% filling rate has less extreme values than the force at a 50% filling rate, which means that the filling rate is the dominant factor that contributes to the value of the surge force. The analysis of the exceedance probability distribution of the hydrodynamic force shows that a 25% filling rate is more effective in terms of sloshing direction as well as structurally safer than a 50% filling rate. These results suggest that the probable extreme of the hydrodynamic forces in random sway is more remarkable than that in random surge.

To obtain a better understanding of the response frequencies, the time histories of the hydrodynamic forces in random motion are converted from the time domain to the frequency domain. This makes it possible to investigate the effect of the frequency component to the hydrodynamic forces induced by the water in random motion, as shown in Fig. 21. According to the response frequency analysis, the surge force is dominated by the resonance frequency of 0.76 Hz, while the sway force and yaw moment are dominated by the 1st and 3rd surge natural frequencies of the tank, as shown in Fig. 21a. The 2nd peak of sway force occurs at 0.98 Hz (1st sway natural frequency). Similarly, the resonance frequency of the surge force in SS4 is in the vicinity of 0.76 Hz, as shown in Fig. 21b. The resonance frequency of the sway force in SS4 is in the vicinity of 0.98 Hz. It is clear that the sway force in random surge is high enough to affect the strength of the tank. Interestingly, the resonance frequencies of the 2nd and 3rd peak frequencies occur at the 3rd sway natural frequency and 1st surge natural frequency. Moreover, the resonance frequency of the 1st and 2nd peak frequency of the yaw moment occurs at the 1st surge natural frequency and 3rd sway natural frequency. Figs. 21c-d show the hydrodynamic force response in random sway at SS3 and SS4 for the 25% filling rate. The resonance frequency of the sway force in SS3 and SS4 are observed in the vicinity of 0.86 Hz, while the resonance frequency of the 1st peak frequency of the surge force and yaw moment in SS3 and SS4 occur at the 3rd surge natural frequency. Interestingly, the resonance frequency of the 2nd peak frequency of the surge force in SS3 occurs at the 1st sway natural frequency, while the resonance frequency of the 2nd peak frequency of the surge force in SS4 occurs at the 1st surge and sway natural frequency. The resonance frequency of the 2nd and 3rd peak frequency of the yaw moment occurs in SS4 at the 1st surge natural frequency and 3rd sway natural frequency.

On the other hand, the surge force is dominated by the resonance frequency of 0.98 Hz, while the sway force is dominated by the resonance frequency of 1.09 Hz for the 50%

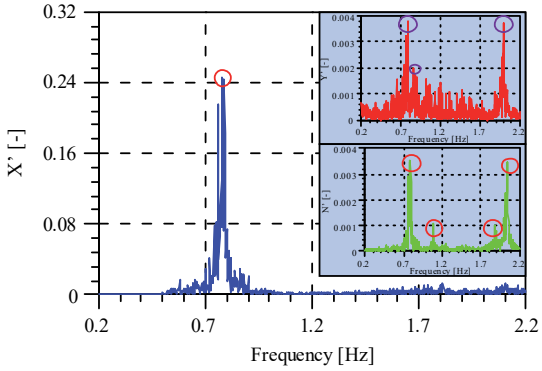

(a) Random surge in SS3 (25% filling rate)

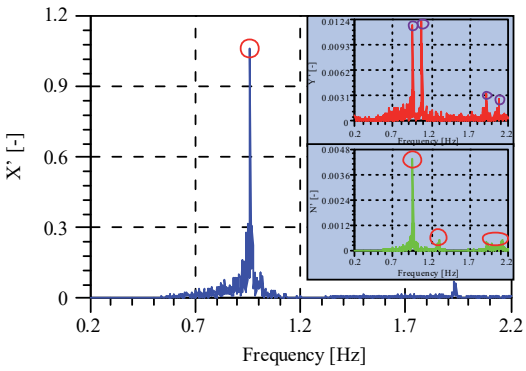

(e) Random surge in SS3 (50% filling rate)

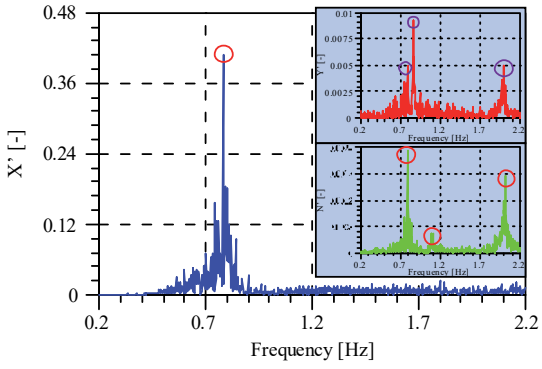

(b) Random surge in SS4 (25% filling rate)

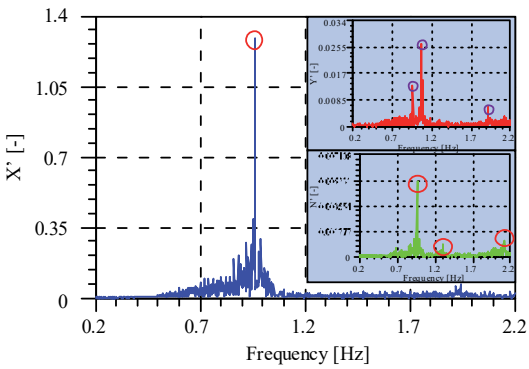

(f) Random surge in SS4 (50% filling rate)

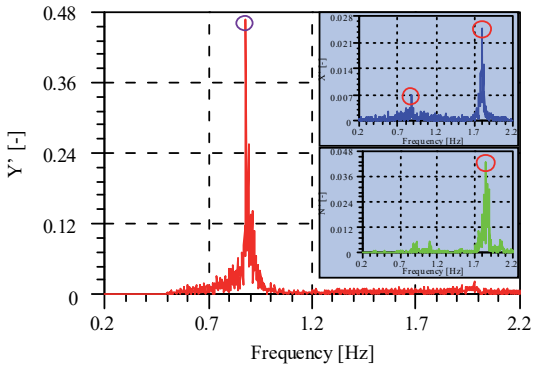

(c) Random sway in SS3 (25% filling rate)

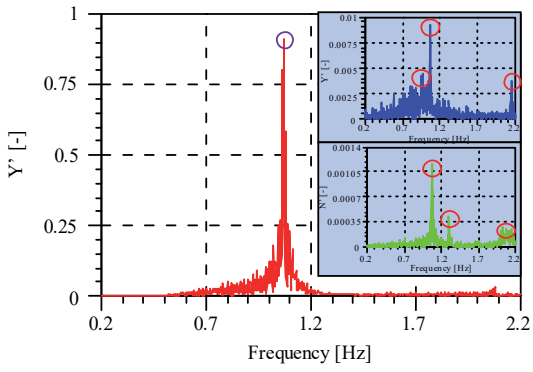

(g) Random sway at SS3 (50% filling rate)

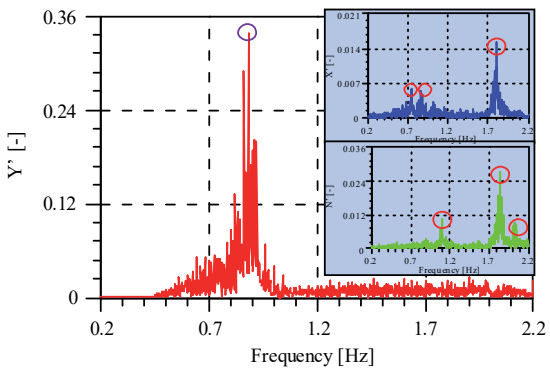

(d) Random sway in SS4 (25% filling rate)

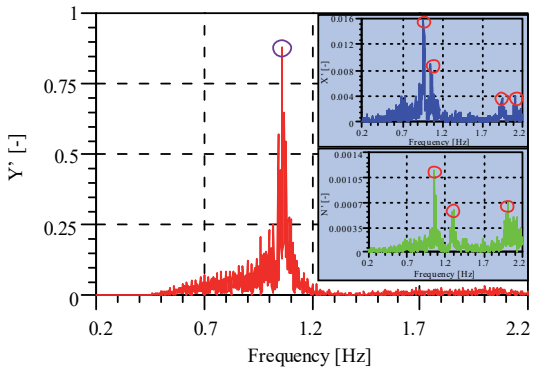

(h) Random sway in SS4 (50% filling rate)

Fig. 21 Hydrodynamic forces response in random motion

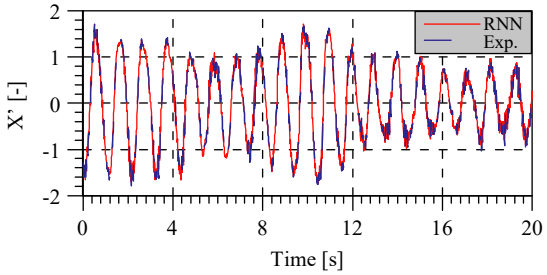

(a) Random surge in SS3 (50% filling rate)

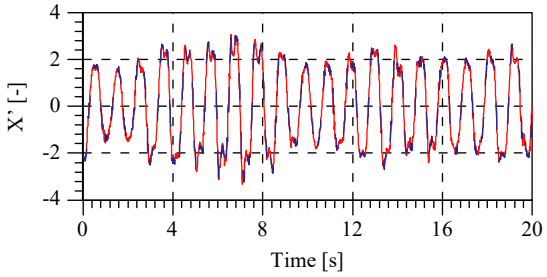

(b) Random surge in SS4 (50% filling rate)

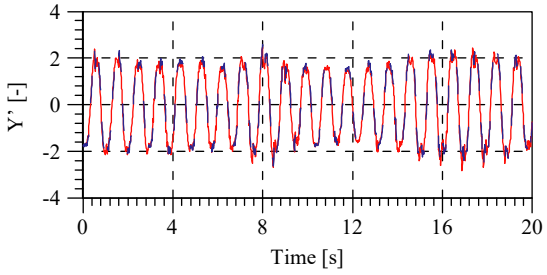

(c) Random sway in SS3 (50% filling rate)

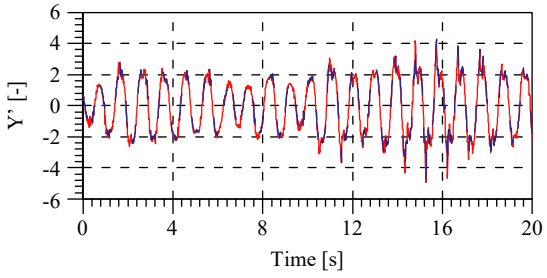

(d) Random sway in SS4 (50% filling rate)

Fig. 22 Comparison of hydrodynamic forces in random motion

filling rate, as shown in Fig. 21e. The 2nd, 3rd and 4th peak of the sway force occur at 0.98, 1.95 and 2.09 Hz, respectively. Similarly, the resonance frequency of the surge force in SS4 is observed in the vicinity of 0.76 Hz, as shown in Fig. 21f. The resonance frequency of the sway force in SS4 for the 50% filling rate is observed in the vicinity of 0.98 Hz. It clear that the sway force in random surge is high enough to affect the strength of the tank. Interestingly, the resonance frequency of the 2nd and 3rd peak frequency occurs at the 3rd sway natural frequency and 1st surge natural frequency. On the other hand, the resonance frequency of the 1st and 2nd peak frequency of the yaw moment occurs at the 1st surge natural frequency and 3rd sway natural frequency. Figs. 21g-h show the resonance frequency of the sway force in SS3 and SS4, which appear in the vicinity of 1.09 Hz. The surge force in SS3 has three peaks, while the surge force in SS4 has four peaks. The 1st, 2nd and 3rd peak of the surge force occur in SS3 at 1.09, 2.09 and 0.98 Hz, respectively. On the other hand, the 1st, 2nd, 3rd and 4th peak of surge force occur in SS4 at 0.98, 1.09, 2.09 and 1.95 Hz, respectively. The resonance frequency of yaw moment in SS3 is the same as that in SS4. These findings confirm that the hydrodynamic forces induced by the liquid are closely related to the natural resonant mode of the tank.

6. RNN estimation of the hydrodynamic forces induced by water

Fig. 22 shows a comparison of the hydrodynamic forces induced by the water between the experiment and RNN estimation in random surge and sway at a 50% filling rate. A good agreement is obtained when the tank is forced into random surge in SS3 and SS4. Figs. 22a-b show that the RNN can predict sloshing load in spite of the variance in excitation frequency and amplitude. The force exerted on the tank is proportional to the strength of the sea condition. The surge force in random surge increases significantly in SS4. Figs. 22c-d show the sway force under various excitations, including SS3 and SS4. The RRN estimation provides a good prediction of the random motions. These results suggest that the RNN can be used to predict the movements of a sloshing load with different excitation motions and sea conditions.

V. CONCLUSIONS

In this paper, a sloshing test of liquid in a 3D membrane tank was conducted using the Stewart platform at Changwon National University and the hydrodynamic forces induced by movement of the liquid inside the 3D membrane tank were investigated. The maximum value of the hydrodynamic force in the direction of the excitation motion remains the same, but it is shifted by the different resonant frequencies of the two filling conditions. The motion of the liquid inside the tank produces different flow phenomena under forced motion conditions, and the effects of various excitation frequencies are made evident by the wave elevation along the tank wall. When the excitation frequency is in the vicinity of the natural frequency of the tank, a wave appears and travels based on the excitation direction of the tank. In this case, the water level increases dramatically and the run-up phenomenon occurs in the tank's corners. Our findings suggest that swirling can occur in the 3D membrane tank that is subjected to forced motion. On the other hand, the tank was forced in random surge and random sway. The hydrodynamic forces induced by the water are analyzed by the hydrodynamic force response in random motion. Very clear effects of the filling rate, excitation direction and sea condition are found in this study. The probable extreme of the hydrodynamic forces induced by the water in

random sway is more remarkable than that in random surge. Exceedance probability is estimated according to the filling rate, sea condition and the extreme hydrodynamic forces based on the statistical analysis. An RNN is used to model the complex dynamics of the sloshing load of liquid in the tank. The RNN predictions of the sloshing load are compared with the experimental results. A new robust modeling approach which can provide the complex dynamics of a sloshing load subject to the random motion of an LNG carrier is developed, which can potentially be applied to simulate the motion of a ship maneuvering in waves.

ACKNOWLEDGEMENT

This research was supported by Basic Science Research Program through the National Research Foundation of Korea (NRF) funded by the Ministry of Science and ICT (2019R1F1A1057551).

REFERENCES

Antuono, M., Bouscasse, B., Colagrossi, A. and Lugni, C (2012). Two-dimensional model method for shallow-water sloshing in rectangular basins. Journal of Fluid Mechanics. Vol. 700, pp. 419-440.

Elahi, R., Fard, M.P. and Javanshir, A (2015). Simulation of liquid sloshing in 2D containers using the volume of fluid method. Ocean Engineering, Vol. 96, pp. 226-244.

Faltinsen, O.M (1978). A numerical nonlinear method of sloshing in tanks with two-dimensional flow. Journal of Ship Research, Vol. 22, No. 3, pp. 193-202.

Faltinsen, O.M and Timokha, A.N (2001). An adaptive multi-model approach to nonlinear in a rectangular tank. Journal of Fluid Mechanics, Vol., 432, pp. 167-200.

Faltinsen, O.M and Timokha, A.N (2002). Asymptotic modal approximation of nonlinear resonant sloshing in a rectangular tank with small fluid depth. Journal of Fluid Mechanics, Vol., 470, pp. 319-357.

Hochreiter, S. and Schmidhuber, J (1997). Long short-term memory. Neural computation, pp. 1735-1870.

Hyeon, J.W., Cho, I.H (2015). Experiment study on sloshing in rectangular tank with vertical porous baffle. Journal of Ocean Engineering and Technology, 291-299.

Hwang, J.H., Kim, I.S., Seo, Y.S, Lee, S.C. and Chon, Y.K (1992). Numerical simulation of liquid sloshing in three-dimensional tanks. Computer & Structures, Vol. 44, pp. 339-342.

ITTC. (2017), "ITTC-Recommended Procedures and Guidelines: Sloshing model test".

Kim, Y (2002). A numerical study on sloshing flows coupled with ship-motion- the anti-rolling tank problem. Journal of Ship Research, Vol. 46, pp. 52-62.

Kim, Y., Nam, B.W., Kim, D.W., Kim, Y.S (2007). Study on coupling effects of ship motion and sloshing. Ocean Engineering, Vol. 34, pp. 2176-2187.

Liu, D.M. and Lin, P.Z (2008). A numerical study of three-dimensional liquid sloshing in tanks. Journal of Computational Physics, Vol. 227, pp. 3921-3939.

Mitra, S., Wang, C.Z., Reddy, J.N. and Khoo, B.C (2012). A 3D fully coupled analysis of nonlinear sloshing and ship motion. Ocean Engineering, Vol. 39, pp. 1-13.

Nasar, T., Sannasiraj, S.A. and Sundar, V (2008). Experimental study of liquid sloshing dynamics in barge carrying tank. Fluid Dynamics Research, Vol. 40, pp. 427-458.

Nam, J.W., Kim, K.S., Hwang, S.C., Heo, J.K., Park, J.C., Kim, M.H (2012). Effect on vessel motion caused by mitigation of sloshing impact load using floaters. Journal of Ocean Engineering and Technology, 50-56.

Sahin, G. and Bayraktar, S (2015). Flow visualization of sloshing in an accelerated two-dimensional rectangular tank. International Journal of Engineering Technologies, Vol. 1, No. 3, pp. 106-112.

Strand, I.M. and Faltinsen, O.M (2017). Linear sloshing in a 2D rectangular tank with a flexible sidewall. Journal of Fluids and Structures, Vol. 73, pp. 70-81.

Wu, C.H., Chen, B.F. and Hung, T.K (2013). Hydrodynamic forces induced by transient sloshing in a 3D rectangular tank due to oblique horizontal excitation. Computers & Mathematics with Applications, Vol. 65, pp. 1163-1186.